Broad Band Shock Associated Noise Modelling for High-Area-Ratio Under-Expanded Jets

V. Gryazev, A. Kalyan, A.P. Markesteijn,[a)] and S.A. Karabasov [a)]

School of Engineering and Material Science, Queen Mary University of London,

Mile End Road, London E1 4NS, United Kingdom

Broadband Shock Associated Noise (BBSAN) is an important component of supersonic jet noise for jets at off-design conditions when the pressure at the nozzle exit is different from the ambient. Two high area ratio under-expanded supersonic jets at Nozzle Pressure Ratios (NPRs) 3.4 and 4.2 are considered. The jets correspond to conditions of the experiment in the Laboratory for Turbulence Research in Aerospace and Combustion (LTRAC) in the Supersonic Jet Facility of Monash University. Flow solutions are obtained by the Large Eddy Simulation (LES) and Reynolds Averaged Navier-Stokes (RANS) methods. The solutions are validated against the Particle Image Velocimetry (PIV) data. For noise spectra predictions, the LES solution is combined with the time-domain Ffowcs Wiliams -Hawkings method. To probe accuracy of the reduced-order method based on acoustic analogy, the RANS solutions are substituted in the Morris and Miller BBSAN method, where different options for modelling of the acoustic correlation scales are investigated. The noise spectra predictions are compared with the experimental data from the non-anechoic LTRAC facility and the NASA empirical sJet model. Apart from the low-frequencies influenced by the jet mixing noise, the RANS-based acoustic predictions align with those from LES for most frequencies in the range of Strouhal numbers (St) $0.4<St<2$ within 1-2 dB.

[a)] Also at GPU-Prime Ltd, 16 St. Thomas Close, Comberton, Cambridge CB23 7DN, United Kingdom

Nomenclature

a_∞ = Speed of sound in the far-field

D_{ef} = Effective jet diameter

D_j = Nozzle exit diameter

M_j = Acoustic Mach number

M_c = Convective Mach number

U_j = Fully expanded jet velocity

U_e = Sonic velocity at the nozzle exit

k_1 = Axial wavenumber component

l = Turbulence length scale in streamwise direction

$l_\perp$ = Turbulence length scale in cross-stream direction

p_s = Shock pressure

p_∞ = Ambient pressure

$\hat{p}_s$ = Fourier transform of shock pressure

R = Distance to the observer

r = Radial coordinate

St = Strouhal number

T_0 = Ambient temperature

$\overline{u}_c$ = Mean convective velocity

$\mathbf{x}$ = Position vector of the observer

$\mathbf{y}$ = Position vector of the source

y_1 = Axial coordinate

ε = Turbulent dissipation rate

θ = Polar angle (observer angle)

κ = Turbulent kinetic energy

τ = Time delay

τ_s = Turbulence time scale

ρ_∞ = Free-stream density

φ = Azimuthal angle

ω = Angular frequency ($2\pi f$)

cov = Covariance

NPR = Nozzle plenum pressure ratio

NTR = Nozzle plenum temperature ratio

I. INTRODUCTION

The pressure mismatch at the nozzle exit develops a series of standing shock waves, or shock-cells in supersonic jets. The interaction between turbulent flow and the shock-cells structure in the jet shear layer is known to generate Broadband Shock Associated Noise (BBSAN). BBSAN is distinctly different to jet mixing noise that occurs due to the turbulence interaction that primarily radiates in the jet downstream direction. Since jet mixing noise masks the shock-associated noise at small angles to the jet flow, it is the upstream direction where the contribution of the shock-associated noise to the overall aircraft noise is most significant. Occasionally, when a feedback occurs between the upstream propagating acoustic waves and the boundary condition at the nozzle lip, there is also a tonal component of the shock-associated noise present, also known as "jet screech".

Various aspects of the shock-associated noise have been a subject of investigation since 1970s experimentally, theoretically, and computationally (Harper-Bourne and Fisher, 1973; Tam, 1975; Zorumski, 1982a, 1982b). Despite the rich history, due to complexity of the underlying fluid mechanics, phenomena that involve high-Reynolds number turbulence and quasi-stationary shock waves whose structure is highly sensitive to the flow conditions, shock-associated noise has remained a fascinating subject for investigation. In addition to the aspects of fundamental fluid mechanics, the study of shock-associated jet noise has an important practical dimension. This type of noise can be a psycho-physiologically important part of the aircraft cabin noise in high altitude conditions when the temperature drops, and the engine fan operates at supersonic off-design conditions (Bodony et al., 2006). Reduction of supersonic jet noise also plays an important role for military aircrafts or during the rocket launches which typically operate at high-thrust conditions since high-levels of acoustic fluctuations are harmful to the personnel exposed to such noise as well as lead to structural fatigue of the aircraft structures (Powell, 1956). Shock-associated noise is also an important factor to avoid in the design of future civil supersonic aircrafts (Cowart, 2013).

For BBSAN modelling, Harper-Bourne and Fisher (1973) considered a series of noise sources which are located along the jet lip-line located at the shock fronts and radiate noise with a phase delay in accordance with turbulence convection speed and the distance between the shock fronts. For calibration of their semi-empirical model, they used pressure measurements obtained with a phased array. The model can correctly capture the main directivity features of the shock-associated noise as well as its fundamental frequencies as a function of the Nozzle Pressure Ratio (NPR) that defines the standing wave pattern and the jet shear layer growth rate in agreement with the earlier studies (Pack, 1950; Davies et al., 1962).

Following the idea of coherent 'large-scale' disturbances interacting with the quasi-periodic standing waves (Pack, 1950), Tam and Tanna (1982) proposed a BBSAN model based on instability waves interacting with the shock-cells, which gives similar predictions of peak frequency compared to the Harper-Bourne and Fisher (1973) model but is much more physics grounded. Based on the stochastic shear layer model (Tam and Chen, 1979), Tam (1987) improved the original shock-associated noise model to take turbulence in the shear layer into account. They considered the solution of the Euler equations that was based on decomposing the flow variables into the background mean-flow, the shock-cell fluctuation, the perturbation due to turbulence, and the perturbation due to the interaction between turbulence and shock-cells. The magnitudes of the standing waves in the model were matched with those of (Pack, 1950). The governing equations were rearranged to Linearized Euler Equations (LEE), which were Fourier transformed and solved with the method of matched asymptotic expansions (van Dyke, 1975). An expression for the far-field noise spectral density was obtained based on the autocorrelation of near-field pressure, where an empirical analytical Gaussian function, the so-called similarity spectrum of the near-field pressure, was used. The underlying assumption was that the noise source spectra have no intrinsic length or time scale. In the follow-on works (Tam and Jackson, 1986; Tam, 1987) the same model was

extended to include the effect of a slowly diverging jet flow, the dissipative effects of the turbulence on the shock-cells, and the effects in slightly heated jets. The last two modifications were based on semi-empirical approaches such as adding viscosity terms to mimic the smoothing out of sharp velocity and density gradients of the shock-cells by turbulence and applying various scaling corrections for the strength of the shock-cell and the far-field noise spectral density.

Building on the semi-empirical models of Tam (1975) and Harper-Bourne (1973), Morris and Miller (2010) developed a BBSAN prediction scheme that is based on the flow decomposition into the constant background flow, the steady shock profile, the unsteady solution component due to the turbulence, and the acoustic component. Using the Lighthill acoustic analogy (Lighthill, 1952, 1954), this formulation rearranges the governing Navier-Stokes equations and consistently takes into account the nozzle geometry and the realistic jet turbulence by solving a two-equation Reynolds Averaged Navier-Stokes (RANS) model numerically. The Morris and Miller model (2010) separates the effects of spatially variable mean-flow velocity gradient from the effective source function that scales with the near-field pressure and reduces the effective source function to the velocity auto-correlation function. The latter is approximated by an analytical Gaussian exponential shape function following Tam and Auriault (1999). Following this approach, the relevant correlation scales and the amplitude of the acoustic source are approximated by turbulence scales obtained from the RANS solution with some calibration parameters based on matching the model predictions to the far-field noise spectra. More recent modifications of the same model make use of frequency-dependent correlation scales for which semi-empirical relations adopted from the jet mixing noise literature were implemented (Miller, 2013). As with the original Tam shock-associated noise model (Tam, 1975), the Morris and Miller (2010) model captures the general shape and the peak of the shock-associated noise well, but tends to under-predict the roll-off of the acoustic spectra at high frequencies. To remedy this, Kalyan and Karabasov (2017) proposed an improved version of the

Morris and Miller (2010) model by including both the turbulence/turbulence interaction and the scatter by the shock wave in the definition of the corresponding acoustic source correlation scales. The Kalyan and Karabasov (2017) model was shown to improve the predictions of the Morris and Miller (2010) model in a number of over-expanded and under-expanded supersonic jet cases.

In addition to the theoretical aeroacoustics methods, the availability of high-resolution methods such as Large Eddy Simulations (LES) for a range of supersonic jet flows opened up another direction in the research of shock-associated jet noise (Paliath and Morris, 2005; Shur et al., 2006; Pineau et al., 2019; Pérez Arroyo et al. 2019a, 2019b). In scale-resolving solutions of the governing Navier-Stokes equations, the shocks, turbulence, and their interaction leading to shock-associated noise are automatically included in the unsteady flow solution. The resulting solutions provide a wealth of space-time resolved data, which can be very useful for validation of theoretical models. Despite making considerable progress in developing accurate algorithms supported by the increased availability of computer power, validation of unsteady flow solutions of supersonic turbulent jets remains highly challenging. This is because supersonic flows are highly sensitive to the jet inflow conditions which are usually not fully reported in experiments. Hence, the motivation of the current work is to partially fulfil this gap by developing a range of computational models for supersonic jet flow cases corresponding to the experiments in the Laboratory for Turbulence Research in Aerospace and Combustion (LTRAC) conducted in the Supersonic Jet Facility of Monash University, Australia (Mitchell et al., 2013; Tan et al., 2019a; Tan et al., 2019b). The LTRAC jets correspond to both the BBSAN and screeching noise behaviour. The jets are well documented for aerodynamics using the high-resolution Particle Image Velocimetry (PIV) measurements and partly for aeroacoustics. In comparison with the existing supersonic jet databases, which have been used for validation of high-resolution flow and noise solutions in the literature (Pérez Arroyo et al. 2019a, 2019b), the convergent nozzle used in the LTRAC experiment has a much higher area ratio. The

resulting strong flow compression at the nozzle exit leads to prominent shock cells not only along the jet centreline but also at the jet lip-line locations. For the highest NPR=4.2 case, the compression and the following expansion waves are so strong that a Mach disk appears downstream of the nozzle exit, which adds an additional challenge for computational modelling.

To simulate the broadband dynamics of the LTRAC jets at NPR=3.4 and 4.2, the high-resolution CABARET LES method accelerated on Graphics Processing Units (GPUs) is used. Following the preliminary work reported in (Markesteijn et al., 2017), the inflow boundary conditions are specified at the nozzle exit (the throat of the convergent nozzle) using the PIV data from the experiment, where sonic condition is assumed. For the far-field spectra predictions, the LES solution is combined with the Ffowcs Williams – Hawkings (FW-H) method following the standard jet noise modelling practice (Ffowcs Williams and Hawkings, 1969; Shur et al., 2005). To investigate the effect of the LES grid sensitivity on flow and noise solution for the most challenging LTRAC NPR=4.2 case, the LES solutions on 3 grid resolutions are obtained and cross-validated in comparison with the available experimental data.

In addition to the LES solutions, the same jet flows are computed using the RANS method based on the $\kappa-\omega$ SST turbulence model. The RANS solutions are used in the acoustic analogy model of Morris and Miller (2010) for far-field noise spectra predictions. The LES- and RANS-based noise spectra predictions, the acoustic results are compared with the available acoustic measurements from the LTRAC facility. Since the experimental facility is known to be non-anechoic, the noise predictions are also validated in comparison with the 'consensus' BBSAN results for the same temperature and nozzle pressure ratio conditions in accordance with the NASA sJet model (Khavaran and Bridges, 2009a, 2009b). The latter is an empirical scaling-law model based on interpolations over a large database of NASA jets of various Mach numbers and temperature ratios. The sJet model includes both the BBSAN and mixing noise components.

II. HIGH-SPEED JET NOISE LTRAC CASE: CONDITIONS, FLOW AND FAR-FIELD MODELING

A. Summary of the experimental set-up

In the LTRAC facility, compressed air is supplied to the plenum chamber at approximately $T_0 = 288K.$ The compressed air is connected directly to the mixing chamber at normal atmospheric conditions where Particle Image Velocimetry (PIV) measurements were taken. The air issues from an axisymmetric nozzle with a blunt lip of 5 mm thickness (Figure 1). The diameter of the nozzle at the exit, D_j is equal to 15mm. The nozzle has an inlet to exit area ratio of 93.44 with a short purely converging section so that the flow is sonic at the exit with a velocity of $U_e = 310\,\mathrm{m/s}$. The converging section consists of a contoured wall with a radius of curvature of $67.15\,\mathrm{mm}$ and a short parallel section at the exit. A complete description of the facility and the PIV system can be found in (Edgington-Mitchell et al., 2014; Tan et al., 2019). The operating conditions of the jets considered in this study are summarised in Table 1.

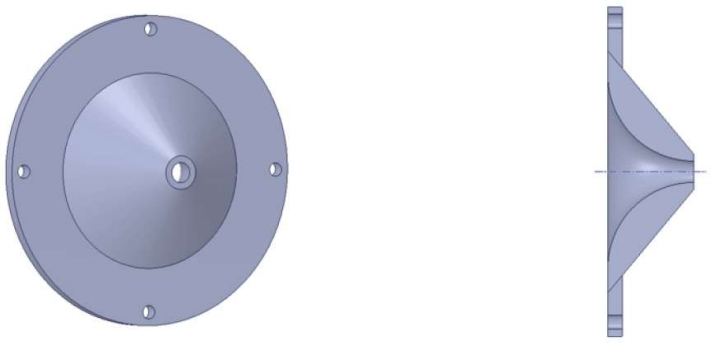

Figure. 1 Rendered views of the CAD model of the LTRAC nozzle (Tan et al. 2019).

TABLE 1. Operating Conditions of the LTRAC jets.

NPR	3.4	4.2

M_j	1.45	1.59
$U_j(m/s)$	412	440
NTR	1	1
$D_{ef}(mm)$	16.02	16.73

In addition to the PIV measurements, acoustic microphone measurements were obtained at several distances from the nozzle exit in the LTRAC experiment. Because of the non-anechoic acoustic facility, the low-frequency part of the noise spectra measured at observer distances from 30 to 100 nozzle diameters (Markesteijn et al., 2017) were shown to not satisfy the standard scaling on R^2, where R is the observer distance from the nozzle exit, for observer angles to the jet flow of 90° and higher (Tan et al. 2016). Hence, the low frequencies of the LTRAC noise spectra are believed to be contaminated by noise not related to BBSAN or jet mixing. At the same time, the mid- to high-frequency noise measurements in the range of relevance to BBSAN remain useful for validation of the jet noise modelling as will be discussed in the following sections.

B. LES modelling

For unsteady simulation of the LTRAC jets, LES are performed and the far-field noise spectra are computed based on the FW-H method with multiple closing discs (Shur et al., 2005). In all simulations, the high-resolution CABARET method (Golovizin and Samarskii, 1998; Karabasov and Golovizin, 2009, Chintagunta et al., 2017) is used for solving the Navier-Stokes equations on unstructured meshes with good preservation of linear wave propagation properties (Tucker and

Karabasov, 2009; Golovizin et al., 2013, Chintagunta et al., 2018). Particular features of the CABARET method include compactness of the computational stencil and asynchronous time stepping for efficient calculations on non-uniform space-time grids (Semiletov and Karabasov, 2013). The CABARET solver was validated for a range of jet flows (Semiletov et al. 2016b; Faranosov et al. 2013). The LES implementation on GPUs further enabled a considerable reduction of the solution time in comparison with conventional LES approaches (Markesteijn and Karabasov, 2018a; Markesteijn and Karabasov, 2018b; Markesteijn and Karabasov, 2019; Markesteijn et al. 2020). The method utilises the so-called split-hexa meshes, which correspond to hanging node-type cells, which are available in the semi-automatic mesh generation process using the OpenFOAM utility "snappyHexMesh" (sHM). This mesh utility enables hexa-dominant mesh generation from triangulated surface geometries (e.g. CAD geometry), which is an essential need for the LES treatment of complex geometries.

In the case of most challenging jet case of NPR=4.2, three LES grids are considered, the details of which are summarised in Table 2. Three regions of specific local grid refinement include the following zones: the jet plume, the region outside of the jet core and in the FW-H surface region. The three non-uniform grids considered correspond to 24, 40, and 70 million cells. For all of them, zones of uniform Cartesian grid cells imbedded in the unstructured snappyHex mesh are generated in the jet shear layer at locations similar to our previous simulations of complex round jet flows (Markesteijn et al. 2020). The mesh containing 40 million cells has a finer resolution in the potential core region than the one having 24 million cells but has a more aggressive grid de-refinement outside of the jet core. The mesh containing 70 million cells is the finest one both in the jet plume and in the FW-H surface region. For the NPR=3.4 case, the intermediate 40 million LES grid is considered.

The simulations are performed on a single computer workstation equipped with 2 GPU cards (NVidia Titan RTX 24GB). For example, in case of the 70 million cells mesh the solution spin-out time is 300 convective Time Units (TU) and a further 1000 TUs are simulated for statistical averaging. Here 1 TU of the simulation corresponds to the time taken by a turbulent eddy travelling at a speed equal to the jet velocity to cover the distance equal to one diameter of the nozzle exit. The total time to solution in this case is 39 hours. This utilises the current solver capability to perform flow and noise predictions using single-precision floating point accuracy without a notable loss in accuracy, due to a modified time-update procedure (Markesteijn and Karabasov, 2018b), as well as the speedup obtained, due to the use of an asynchronous time stepping algorithm. In accordance with the latter algorithm, the cells of the LES grid are distributed into several groups, which are updated at different rates depending on the cell size in accordance with an approximately constant local Courant-Friedrichs-Lewy (CFL) number, which is kept as close to the optimal as possible. It can be noted that the optimal CFL number for CABARET is 0.5; this is where the scheme becomes exact for one-dimensional linear wave propagation. For the time stepping, 7 dyadic update groups are used, where the local time step changes from Δt to $64\Delta t$, and where Δt is the minimum time step.

Details of the three LES grids and the corresponding times to solution of the GPU LES solver accelerated on 2 NVidia Titan RTX cards are summarised in Table 2. The maximum frequency resolution on the grid corresponding to 8 points per wavelengths (p.p.w.) is defined in terms of the dimensionless Strouhal number $St = fD_j / U_j$, which is based on the fully expanded jet velocity U_j and the nozzle exit diameter D_j

TABLE 2. LES grid details.

Grid	24 million cells	40 million cells	70 million cells

Mesh resolution at the nozzle lip $\Delta x / D_j \sim \Delta y / D_j \sim \Delta z / D_j =$	0.04	0.0267	0.0267
Mesh resolution at the nozzle exit region of the FW-H surface and the maximum frequency resolved based on 8 ppw. $\Delta x / D_j \sim \Delta y / D_j \sim \Delta z / D_j =$	0.08 St = 1.7	0.107 St = 1.3	0.053 St = 2.6
Mesh resolution at the end closing disc region of the FW-H surface and the maximum frequency resolved based on 8 ppw. $\Delta x / D_j \sim \Delta y / D_j \sim \Delta z / D_j =$	0.107 St = 1.3	0.16 St = 0.86	0.08 St = 1.7
Mesh resolution at the nozzle lip $\Delta x / D_j \sim \Delta y / D_j \sim \Delta z / D_j =$	0.04	0.0267	0.0267
Simulation run times, amount of TUs generated and the total time to solution	300 TUs (spin-out) + 1200 TUs (averaging), 20 hours	400 TUs (spin out) + 800 TUs (averaging), 26 hours	300 TUs (spin-out) + 1000 TUs (averaging), 39 hours

C. RANS modelling

Following (Tan et al., 2019a), the RANS solutions of the same LTRAC jets were obtained using the $\kappa-\omega$ SST turbulence model, which includes the compressibility corrections and accounts for the adverse pressure gradients typical of supersonic flows. The 3D axisymmetric RANS equations are

solved with imposing an inlet boundary condition at the inflow region of the nozzle, free-stream boundary conditions at the far-field domains, and a downstream pressure condition for the jet outflow. The computational domain is designed to be sufficiently large to ensure that numerical open boundary condition effect is negligible. RANS calculations were carried out on several initial coarse grids corresponding to a range of computational domain sizes, 60-100 nozzle diameters axially and 20-40 nozzle diameters radially to ensure that the pressure and Mach number profiles in the jet core region remain virtually insensitive to the domain size. Away from the jet flow region, the grid is kept coarse to optimize the total grid count. Grid refinement was carried out by iteratively running several RANS calculations to verify that the target y^+ value in the wall-normal units is close to 1 as recommended in the literature. The final computational mesh includes $165 \cdot 10^3$ elements and extends $60D_j$ and $20D_j$, in axial and transverse dimensions respectively. The governing RANS equations are solved using the density-based solver in ANSYS Fluent. For spatial discretization, a second-order Roe scheme is used and an implicit integration scheme in time. The iterations are stopped when the solution residuals reduce to 10^{-5} of the initial values.

D. Flow-field comparison with experiment

The flow modelling results of the NPR = 3.4 (40 million cell LES grid) and NPR = 4.2 jets (24 and 70 million cell LES grid) are presented in this section. For comparing different datasets, the velocities and distances are normalised on nozzle diameter D_j and jet exit velocity U_e.

1. NPR = 3.4 jet

Figure 2 compares the distributions of the mean axial velocity component from the LES and the PIV data in the jet symmetry plane. A detailed comparison of LES and RANS solutions with the PIV data is presented in Figs. 3-4, which show the distributions of the time-averaged axial velocity

and turbulent kinetic energy along jet centreline and lip-line $(r/D_j = 0.5)$ locations. Notably, the LES and RANS time-averaged velocity solutions are in good agreement with the experiment: the location and the amplitude of the first 4-5 shock-cells are well predicted (Fig.3a). On the one hand, the LES solution more accurately captures the jet velocity profile in comparison with the RANS solution especially for the centreline distribution. On the other hand, the LES solution tends to over-amplify the turbulent kinetic energy distribution (especially the first prominent peak) in comparison with the RANS solution for the jet lip-line locations (Fig.4b), which may be related to the initially laminar inflow condition effect in the LES simulation. At the same time, the RANS solutions fail to resolve any turbulence along the jet centreline (Fig.3b) as typical for the RANS models, where the turbulence generation is related to the mean-flow vorticity, and which can be regarded as general deficiency of RANS models.

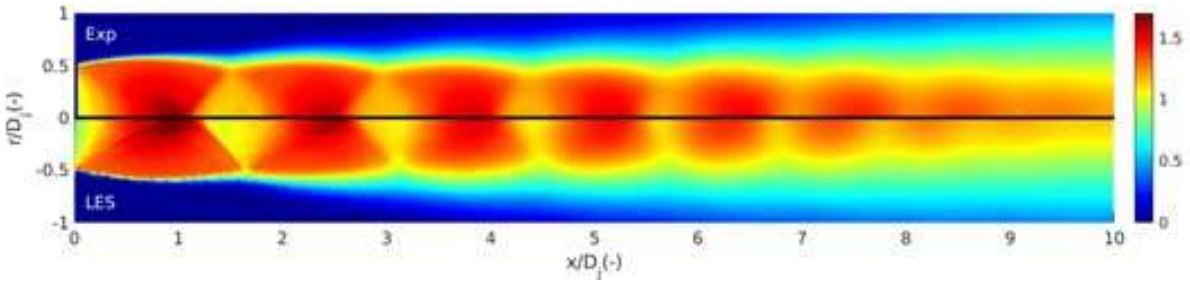

(a)

FIG. 2. Comparison of the LES solution (bottom half) with the PIV data (top half) for the NPR=3.4 jet: axial mean-flow velocity normalised by jet exit velocity.

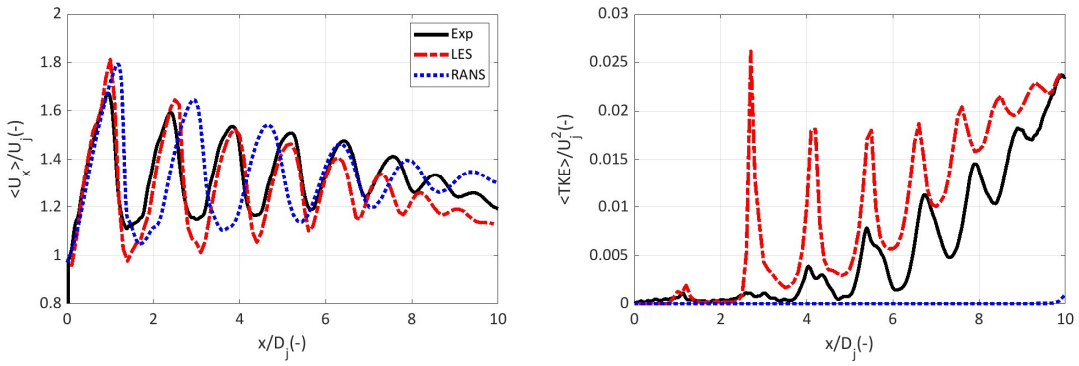

(a) (b)

FIG. 3. Comparison of the LES and RANS solutions along the jet centreline versus the PIV data for the NPR=3.4 jet: axial mean-flow velocity distributions (a) and turbulent kinetic energy (b)

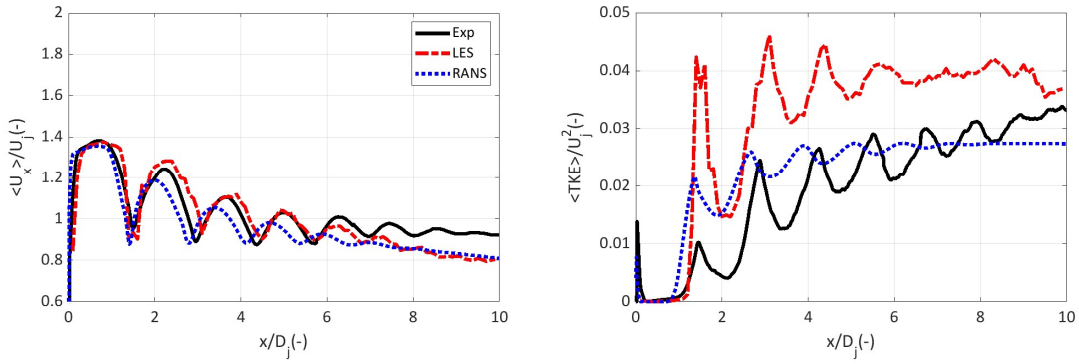

(a) (b)

FIG. 4. Comparison of the LES and RANS solution along the jet lip-line versus the PIV data for the NPR=3.4 jet: axial mean-flow velocity distributions (a) and turbulent kinetic energy (b)

2. NPR = 4.2 jet

The fastest LTRAC jet of NPR = 4.2 corresponds to a strong expansion, which generates shock-cells in the entire jet extending to the jet lip-line locations as well as a Mach disk downstream of the nozzle exit. The latter features typical of strongly under-expanded jets are often missing in the

laboratory-scale experiments, such as the jet case at a relatively low NPR = 2.27 recently considered by (Pérez Arroyo et al. 2019a).

Figs. 5 and 6 compare the 2D distributions of the time-averaged axial velocity component and turbulent kinetic energy of the LES solutions on the 2 grids in the jet symmetry plane with the PIV data. It can be noted that both the coarse- and fine- grid LES solution correctly capture the location of the first 4 shock-cells as well as the Mack disk. The LES solution on the 70 million cell grid leads to a notable improvement of the turbulent kinetic energy distribution in comparison with the 24 million LES grid solution (Fig.6b). The latter shows a strong amplification of the turbulent kinetic energy levels on the coarse grid due to the lack of the mesh resolution in the shear layers thereby leading to insufficient turbulent mixing.

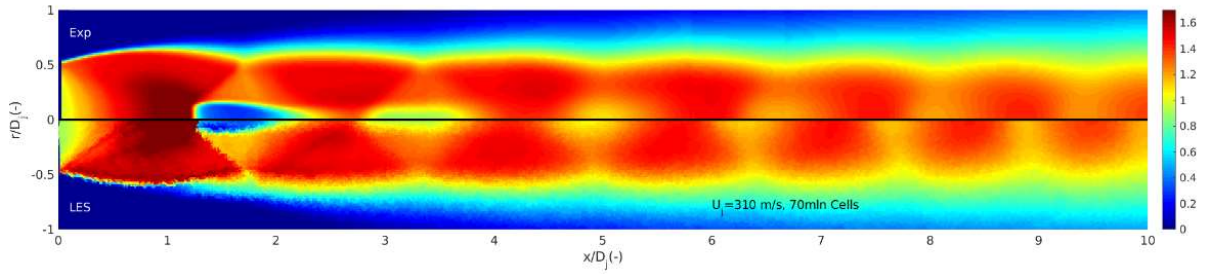

(a)

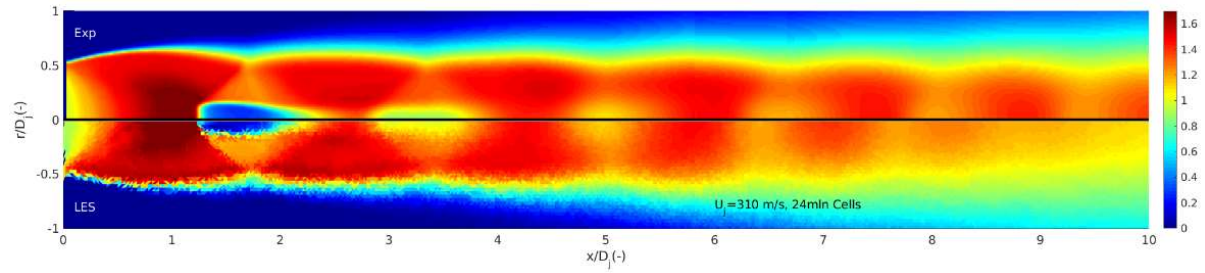

(b)

FIG. 5. Comparison of the LES solution (bottom half) with the PIV data (top half) for the NPR=4.2 jet: axial mean-flow velocity normalised by jet exit velocity for 70 million mesh (a) and 24 million mesh (b).

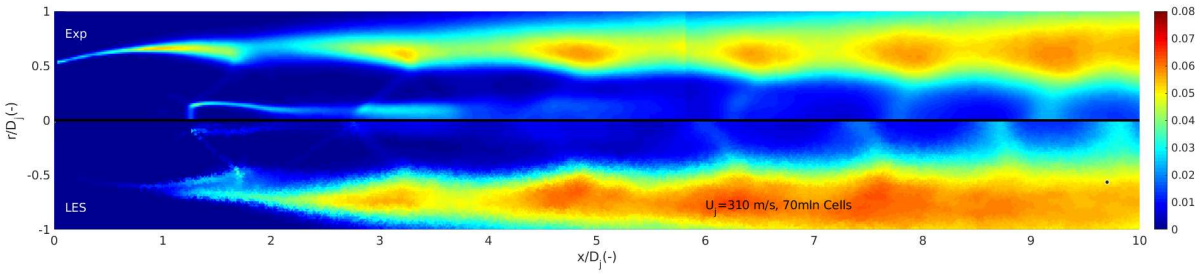

(a)

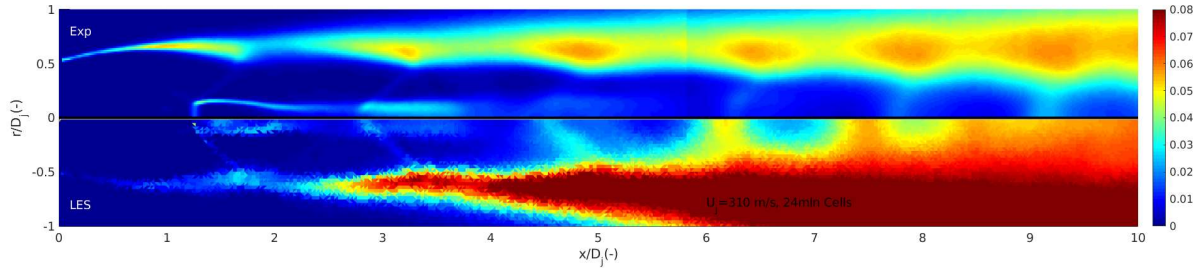

(b)

FIG. 6. Comparison of the LES solution (bottom half) with the PIV data (top half) for the NPR=4.2 jet: turbulent kinetic energy normalised by U_e^2 for 70 million mesh (a) and 24 million mesh (b).

Figs. 7 and 8 compare the jet centreline time-averaged axial velocity and turbulent kinetic energy distributions of the LES solutions on the 24 and 70 million meshes with the RANS solutions and with the experiment.

Both the LES solutions capture the mean-flow velocity distributions in amplitude and phase in comparison with the PIV data up to the 4th shock cell (Fig.7a). For further shock-cells, no. 5 and 6, the fine grid LES solutions still preserves the correct amplitude of the shock-cells in comparison with the experiment while the phase error of up to 50% is accumulated.

The RANS solution captures the Mach disk correctly but under-predicts the potential core of the jet, which is especially notable for the centreline jet location where the shock-cell- structure predicted by RANS is very different from the experiment (Fig.7a).

The LES solution of turbulent kinetic energy on the 70 million grid is in encouraging agreement with the experiment. Recalling that the jet core resolution of the 70 million mesh is the same as the 40 million mesh, it can be suggested that initially laminar flow condition is less of a problem for the fastest NPR=4.2 case in comparison with the NPR=3.4 case (compare Figs.7b and 8b with Figs. 3b and 4b). This can be attributed to a thinner boundary layer and a faster transition to turbulence, which can be expected in the faster NPR = 4.2 jet in comparison with the NPR = 3.4 jet.

Still, the RANS solution of the turbulent kinetic energy distribution along the lip-line is closer to the experiment in comparison with the LES solution on the fine 70 million grid (Fig.8b), which suggests that the latter LES grid needs to be further refined to correctly resolve the turbulent mixing.

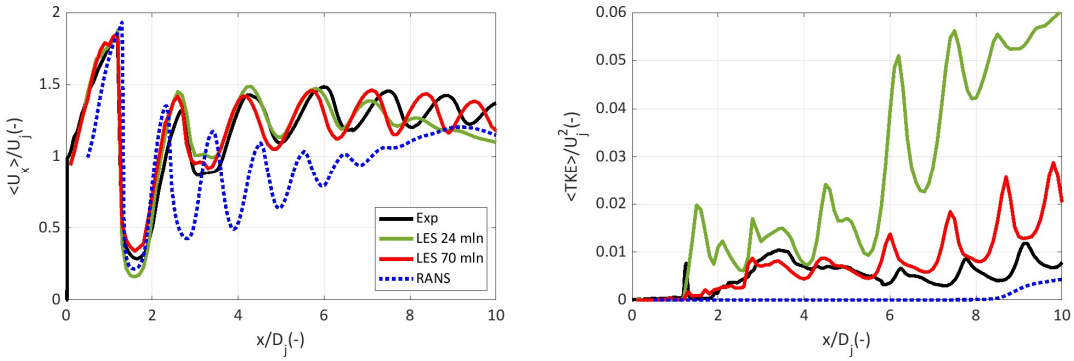

(a) (b)

FIG. 7. Comparison of the LES and RANS solutions along the jet centreline versus the PIV data for the NPR=4.2 jet: axial mean-flow velocity distributions (a) and turbulent kinetic energy (b)

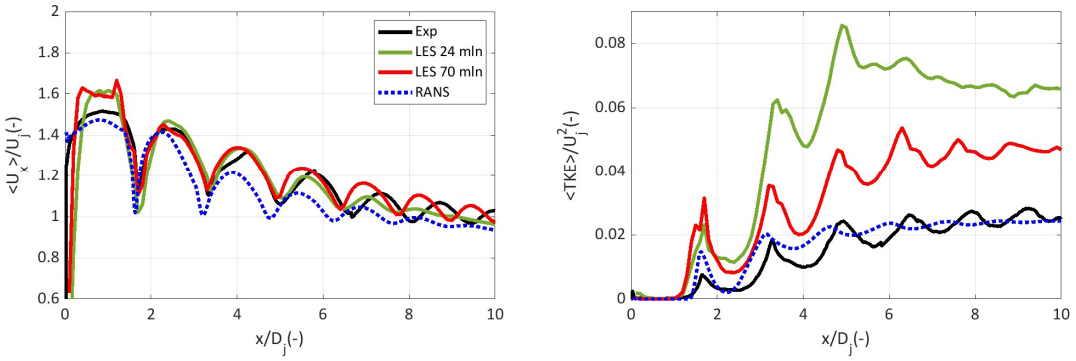

(a) (b)

FIG. 8. Comparison of the LES and RANS solutions along the jet lip-line versus the PIV data for the NPR=4.2 jet: axial mean-flow velocity distributions (a) and turbulent kinetic energy (b)

E. Far-field acoustic modelling

1. FW-H method based on LES solution

For far-field noise spectra computation, the LES solution is combined with the time-domain Ffowcs Williams –Hawkings (1969) (FW-H) method based on a permeable acoustic integration surface of a funnel shape. The control surface includes 16 closing discs over which the signal is averaged to reduce the pseudo-sound effects (Shur et al., 2005; Semiletov et al., 2016). The acoustic signal is computed at the distance of the acoustic microphone used in the experiment $(R/D_j = 100)$. The time-domain pressure signal is Fourier transformed using the single-sided spectra definition and the resulting sound pressure Power Spectral Density (PSD) is computed using the Welch method, the details of which can be found in (Semiletov and Karabasov, 2018). The common definition of PSD is used with 1Hz reference frequency and 20μPa reference pressure.

2. Acoustic analogy method based on the RANS solution

Following (Morris and Miller, 2010) and (Kalyan and Karabasov, 2017), the RANS-based acoustic analogy model of BBSAN is implemented. First, by ignoring the mean-flow sound propagation effect for angles of interest with respect to BBSAN that are close to 90°, the governing Navier-Stokes equations are rearranged to the homogeneous linear wave propagation form:

$$\frac{\partial \pi'}{\partial t} + \frac{\partial v_i'}{\partial y_i} = 0$$

$$\frac{\partial v_i'}{\partial t} + \bar{a}^2 \frac{\partial \pi'}{\partial y_i} = f_i^v \qquad (1)$$

$$i.j = 1,2,3,$$

where,

$$f_i^v = -v_{sj} \frac{\partial v_{ti}}{\partial y_j} - v_{tj} \frac{\partial v_{si}}{\partial y_j}, \qquad (2)$$

is the unsteady force per unit volume associated with interactions between the shock and turbulent velocity fluctuations. The latter scales with the shock pressure and the unsteady velocity fluctuations, $f_i^v \sim p_s v_t / \rho_\infty a_\infty l$. The shock pressure is defined as the difference between the local static pressure and the ambient,

$$p_s(y) = p(y) - p_\infty(y) \qquad (3)$$

The acoustic propagation equations are solved analytically using the free-space Green's function method. A cylindrical-polar coordinate system $y = (x, r\cos\phi, r\sin\phi)$ is considered and is schematically illustrated in Figure 9.

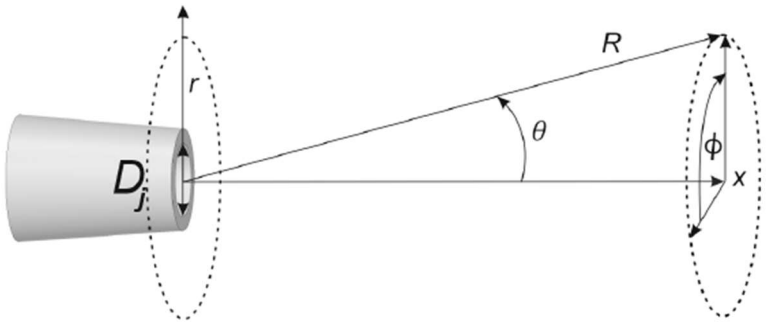

FIG 9. Definition of the cylindrical-polar coordinate system.

By making use of the Proudman form (Proudman, 1952) for the cross-correlation, the expression for the far-field sound power spectral density is derived:

$$S(\mathbf{x},\omega)=\frac{\omega^2}{16\pi^2 a_\infty^4 |\mathbf{x}|^2}\int_{-\infty}^{\infty}\int_{-\infty}^{\infty}\int_{-\infty}^{\infty}\frac{1}{l^2}p_s(\mathbf{y})p_s(\mathbf{y}+\boldsymbol{\eta})R^v(\mathbf{y},\boldsymbol{\eta},\tau)\exp\left[i\omega(\tau-\frac{\mathbf{x}\boldsymbol{\eta}}{a_\infty|\mathbf{x}|})\right]d\tau d\boldsymbol{\eta} d\mathbf{y}, \tag{4}$$

and where

$$R^v(\mathbf{y},\Delta,\tau)=\overline{v_{t2}(\mathbf{y},t)v_{t2}(\mathbf{y}+\boldsymbol{\eta},t+\tau)}, \tag{5}$$

is the near-field velocity auto-covariance function, which is modelled in accordance with the analytical Gaussian/exponential shape function (Tam and Auriault, 1999):

$$R^v(\mathbf{y},\boldsymbol{\eta},\tau)\approx R^v(\mathbf{y},0,0)\exp\left[-\frac{|\tau|}{\tau_s}\right]\exp\left[-\frac{(\boldsymbol{\eta}_1-\bar{u}_c\tau)^2}{l^2}\right]\exp\left[\frac{-(\boldsymbol{\eta}_2^2+\boldsymbol{\eta}_3^2)^2}{l_\perp}\right]. \tag{6}$$

In the above equation, $\boldsymbol{\eta}_1$ is the Cartesian coordinate in the stream-wise (jet flow) direction, $(\boldsymbol{\eta}_2,\boldsymbol{\eta}_3)$ are in the transverse plane, $(\boldsymbol{\eta}_1,\boldsymbol{\eta}_2)$ are in-plane with the far-field observer, $\bar{u}_c$ is a characteristic turbulence convection speed, which can be scaled with the jet velocity at the nozzle exit, U_e, via a proportionality coefficient, $\alpha_c=0.7-0.8$. It can be noted that both the considered LTRAC jets are under-expanded, hence, the equivalent convection speed scaling based on the fully expanded jet velocity, which is 30-40% greater than the jet velocity at the nozzle exit, would be in

the range of 0.5-0.6, and which is in a reasonable agreement with the jet mixing noise literature (Harper-Bourne, 2003; Semiletov and Karabasov, 2018). To close the acoustic model, the convective Mach number is defined as $\mathrm{M_c} = \overline{\mathrm{u}}_\mathrm{c} / \mathrm{a}_\infty$, where the acoustic Mach number $\mathrm{M_j} = \mathrm{U_e} / \mathrm{a}_\infty$ is based on the sonic velocity at the nozzle exit.

By evaluating the inner integral over τ analytically, the acoustic integral reduces to:

$$\begin{aligned} \mathrm{S}(\mathbf{x},\omega) = \frac{1}{16\pi\sqrt{\pi}\,\mathrm{a}_\infty^4 \mathrm{R}^2} \int_{-\infty}^{\infty}\int_{-\infty}^{\infty}\int_{-\infty}^{\infty} \frac{\mathrm{c_A}\kappa \mathrm{l}_\perp^2}{\mathrm{l}\tau_\mathrm{s}} \mathrm{p_s}(\mathbf{y})\hat{\mathrm{p}}_\mathrm{s}(\mathrm{k}_1,\mathrm{y}_2,\mathrm{y}_3)\exp(\mathrm{i}\mathrm{k}_1\mathrm{y}_1) \\ \times \frac{\tau_\mathrm{s}^2\omega^2 \exp[-\mathrm{l}^2(\mathrm{k}_1-\omega\cos\theta/\mathrm{a}_\infty)^2/4 - \omega^2\mathrm{l}_\perp^2\sin^2\theta/4\mathrm{a}_\infty^2]}{1+(1-\mathrm{M_c}\cos\theta+\overline{\mathrm{u}}_\mathrm{c}\mathrm{k}_1/\omega)^2\omega^2\tau_\mathrm{s}^2} \mathrm{d}\mathrm{k}_1\mathrm{d}\mathbf{y}, \end{aligned} \tag{7}$$

where, k_1 is the axial wavenumber component and $\hat{\mathrm{p}}_\mathrm{s}$ is the wave-number transform of $\mathrm{p_s}$ in the stream-wise direction.

The temporal correlation scale of τ_s and the spatial correlation scales of $\mathrm{l}_\perp$ and l, which partly capture the anisotropy effect, are evaluated as the corresponding integral scales of the velocity auto-correlation function $\mathrm{R^v}(\mathbf{y},\Delta,\tau) = \overline{\mathrm{v_{t2}}(\mathbf{y},\mathrm{t})\mathrm{v_{t2}}(\mathbf{y}+\Delta,\mathrm{t}+\tau)}$. In the framework of RANS modelling, the correlation scales are modelled by assuming a linear relationship between the integral scales and some characteristic flow scale in the turbulent jet flow. For example, in the Morris and Miller (2010) model, following the jet mixing noise model (Tam and Auriault, 1999), the turbulent length and time scales are modelled dimensionally and are related to the large scales from equating the rate of energy production at the large scales to the rate of viscous dissipation at the smallest scales

That is,

$$\tau_\mathrm{s} = \mathrm{c}_\tau \frac{\kappa}{\varepsilon}, \quad \mathrm{l} = \mathrm{c}_\mathrm{l} \frac{\kappa^{3/2}}{\varepsilon}, \quad \mathrm{l}_\perp = \mathrm{c}_\perp \mathrm{l}, \tag{8}$$

and

$$R^{v}(\mathbf{y},0,0)=\overline{v_{t2}(\mathbf{y},t)^{2}}=c_{A}\kappa, \tag{9}$$

where κ and ε are the turbulence kinetic energy and the dissipation rate obtained from the RANS solution, and $c_{l}, c_{\perp}, c_{\tau}$ and c_{A} are some calibration parameters. The calibration parameters are obtained by fitting the model predictions to the reference far-field noise spectrum measurements for one jet condition and one observer angle to the jet flow (and then keeping the same parameters for all other observer angles and jet conditions). In the current LTRAC cases, we have used the NASA sJet model (Khavaran and Bridges, 2009a, 2009b) for the reference noise spectrum of the NPR=3.4 jet at 90° angle. The resulting values of the model constants are given below:

$$c_{l}=2.9,\quad c_{\perp}=0.3,\quad c_{\tau}=0.5,\quad c_{A}=0.5. \tag{10}$$

Additionally, following the two-scale model of Kalyan and Karabasov (2017), two mechanisms of shock-associated noise are considered. One corresponds to a jet-mixing-noise like process and has the time correlation scale τ_{s1}, which scales with turbulence energy dissipation rate (same as in the Morris and Miller (2010) model), and the other corresponds to the acoustic scattering of turbulent eddies by the shock-cell, which has the time correlation scale τ_{s2} that depends on the stream-wise mean-flow velocity gradient. Then, the resulting correlation time scale is given by (Ghahramani, 2005):

$$\tau_{s}=\tau_{s1}\cdot f(\tau_{s1},\tau_{s2}), \tag{11}$$

where, the function

$$f(\tau_{s1},\tau_{s2})=\sqrt{1+\left(\frac{\tau_{s1}}{\tau_{s2}}\right)^{2}+\frac{\mathrm{cov}\left(X(\tau_{s1}),Y(\tau_{s2})\right)}{{\tau_{s1}}^{2}}} \tag{12}$$

is approximated by a model based on the dimensional analysis

$$\mathrm{f}(\tau_{s1},\tau_{s2})=\left(\frac{\tau_{s1}}{\tau_{s2}}\right)^{\alpha} \quad \text{if} \quad \frac{\tau_{s1}}{\tau_{s2}}>1 \quad \text{and} \quad \mathrm{f}(\tau_{s1},\tau_{s2})=1, \ \text{otherwise,} \tag{13}$$

where, α is a model parameter that needs to be specified along with the rest of the space and time scale functions similar to the Morris and Miller model (2010),

$$\tau_{s1}=\frac{\mathrm{c}_{\tau}\kappa(\mathbf{y})}{\varepsilon(\mathbf{y})}, \quad \tau_{s2}=\mathrm{c}_{\tau}\left|\frac{\partial\overline{\mathrm{v}}_1(\mathbf{y})}{\partial \mathrm{y}_1}\right|^{-1}, \quad \mathrm{l}=\mathrm{c}_{\mathrm{l}}\sqrt{\kappa(\mathbf{y})}\tau_{s}(\mathbf{y}), \quad \mathrm{l}_{\perp}=\mathrm{c}_{\perp}\mathrm{l}(\mathbf{y}). \tag{14}$$

So, for example, for $\tau_{s1}/\tau_{s2}>1$, the effect associated with the acoustic scattering of turbulent eddies by the shock-cell is neglected in comparison with the turbulent energy dissipation, and the Kalyan and Karabasov (2017) model automatically switches to the Morris and Miller (2010) model.

To obtain the Fourier transform of the shock pressure, $\hat{\mathrm{p}}_s$, the RANS flow domain is symmetrically extended to the negative y_1-coordinate region (x-coordinate in the Cartesian-polar coordinate system) with respect to $\mathrm{x}=0$. The numerical Fourier transform in stream-wise direction is computed with a Hanning window applied to minimize the finite computational domain effect. Before integration, the RANS solution is interpolated to a uniform Cartesian grid in $(\mathrm{x}-\mathrm{r})$ plane. Fig.10a shows one-half of the acoustic integration domain (the physical solution domain corresponding to $\mathrm{y}_1>0$) and the Fourier domain (Fig.10b) used in the spectral part of the acoustic model.

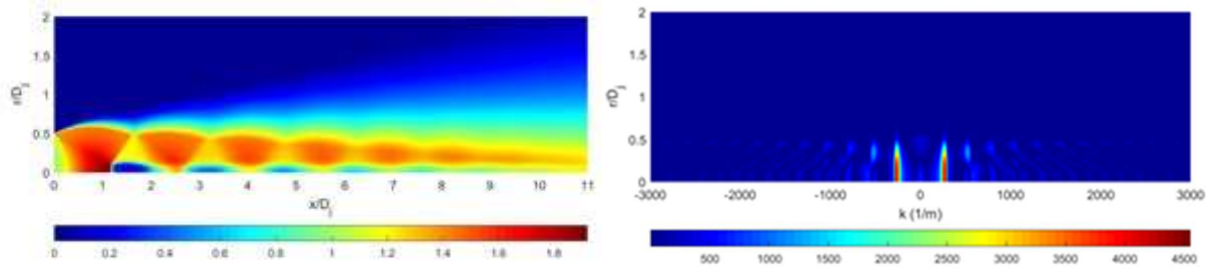

(a) (b)

FIG. 10. The acoustic integration part of the RANS simulation domain of the NPR = 4.2 jet case: the physical domain showing contours of the mean-flow axial jet velocity normalised by U_j (a) and the Fourier domain showing the shock pressure magnitude, $|\hat{p}_s|$ from 0 to $0.45p_\infty$ (b).

To investigate the importance of the two BBSAN mechanisms for the LTRAC jets, the jet lip-line distribution of the characteristic scale ratio $\frac{\tau_{s1}}{\tau_{s2}} = \frac{\kappa(\mathbf{y})}{\varepsilon(\mathbf{y})}\left|\frac{\partial \overline{v}_1(\mathbf{y})}{\partial y_1}\right|$ is computed for both LTRAC jet cases (Fig.11). The RANS solutions are compared with the PIV data on the same plots. Notably, in both the cases $\tau_{s1}/\tau_{s2} < 1$, which means that the turbulent energy dissipation is the dominant mechanism defining the correlation time and length scales for these jets, hence, making the original Morris and Miller (2010) model applicable for the considered jet cases.

It can be noted that the complete dominance of the turbulence dissipation mechanism in acoustic scales makes the LTRAC jets different in comparison with the convergent and convergent-divergent PSU (Pennsylvania State University) jet cases (Morris and Miller, 2010). For the PSU jets, (Kalyan and Karabasov, 2017) reported a large region of $\tau_{s1}/\tau_{s2} > 1$ along the jet lip-line, which corresponds to the turbulent eddy/shock-cell scattering process. It can be hypothesised that the difference between the LTRAC and PSU jets is due to the strong screeching component of the LTRAC jets, which effectively (in the time-average sense) diffuses the jet shear layers thereby reducing the mean-flow velocity gradients.

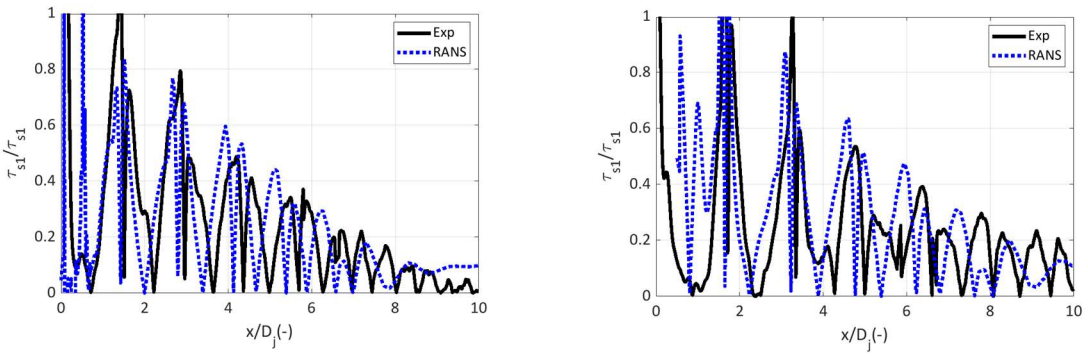

(a) (b)

FIG. 11. Jet lip-line distributions of the dimensionless function τ_{s1}/τ_{s2}, which detects the zones of importance of the shock-scattering mechanism in BBSAN $(\tau_{s1}/\tau_{s2})>1$ for the LTRAC jets corresponding to NPR=3.4 (a) and NPR=4.2 (b). Both the PIV data and the RANS solutions predict the dominance of the turbulence dissipation mechanism for the LTRAC jets.

3. Comparison with far-field noise measurements

Figs.12 and 14 show the far-field noise power spectra density predictions based on the LES solution coupled with FW-H method for the NPR=3.4 jet on the 40 million grid and the NPR=4.2 jet on the 70 million grid. All LES-FW-H model predictions are compared with the RANS-based Morris and Miller (2010) BBSAN model, the results of the NASA empirical sJet model (Khavaran and Bridges, 2009a; 2009b), and the LTRAC acoustic measurements. The noise spectra correspond to 90° and 120° observer angles, which are most typical of the BBSAN component of supersonic jet noise. All acoustic data are presented at the observer distance of 100 nozzle diameters from the nozzle exit. For the most challenging NPR = 4.2 jet case, the far-field spectra predictions are computed using three LES grids (24, 40, and 70 million cells) and compared with the experiment (Fig.13).

First, it can be noted that the noise spectra predictions of the LES-FW-H models are within 1-2dB from the RANS-based predictions for the NPR = 3.4 and 4.2 over the high frequency range

corresponding to $0.6 < St < 2$ (Figs. 12 and 14). For the 70 million grid for the NPR = 4.2, the LES-FW-H solution is also within 2-3dB from the LTRAC experiment for the same range of high frequencies. For frequencies higher than St = 2, the LES-FW-H solutions are under-resolved, while the LTRAC acoustic measurements show a faster drop off in comparison with the NASA sJet model predictions. This is because, in contrast to the LTRAC measurements, the sJet model includes a correction for atmospheric attenuation.

For low-frequencies ($0.04 < St < 0.5$), where the LTRAC data are contaminated by noise, the LES-FW-H solution is within 2-3dB from the reference NASA sJet solution.

In addition, the LES correctly captures the screech tone frequencies of the experiment of St = 0.6 and St = 0.9 for the 90^o spectrum of the NPR = 3.4 LTRAC jet and also those of St = 0.2 and St = 0.9 for the 120^o spectrum of the same jet. Furthermore, the LES-FW-H solution of the NPR = 4.2 LTRAC jet resolves the screech tone frequency of St = 0.4 for both the 90^o and 120^o observer angles.

It can also be noticed, as the grid resolution increases from 24 million to 70 million cells, the predictions of the LES-FW-H model of the NPR = 4.2 jet for high frequencies gradually approach the LTRAC experiment spectra (Fig.13).

The RANS-based BBSAN model predictions at frequencies lower than 0.7 for the 90^o observer angle fall off more rapidly than the LES and the sJet spectra. This can be explained by the jet mixing noise contribution, which is not accounted for in the pure BBSAN acoustic analogy model.

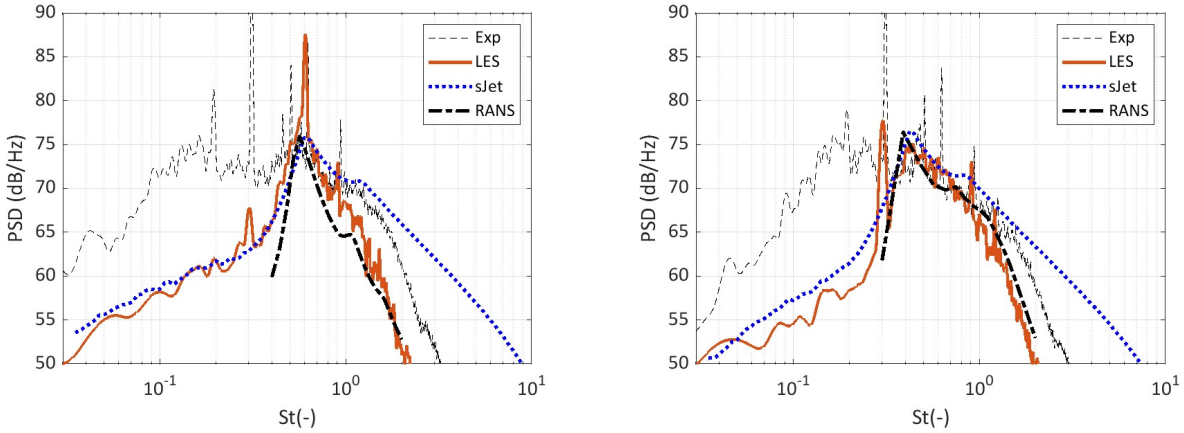

FIG. 12. Comparison of the Power Spectra Density predictions of the LES-FW-H and RANS-based acoustic models with the NASA sJet model and the LTRAC experiment for the NPR = 3.4 at 90° (a) and 120° (b) observer angles.

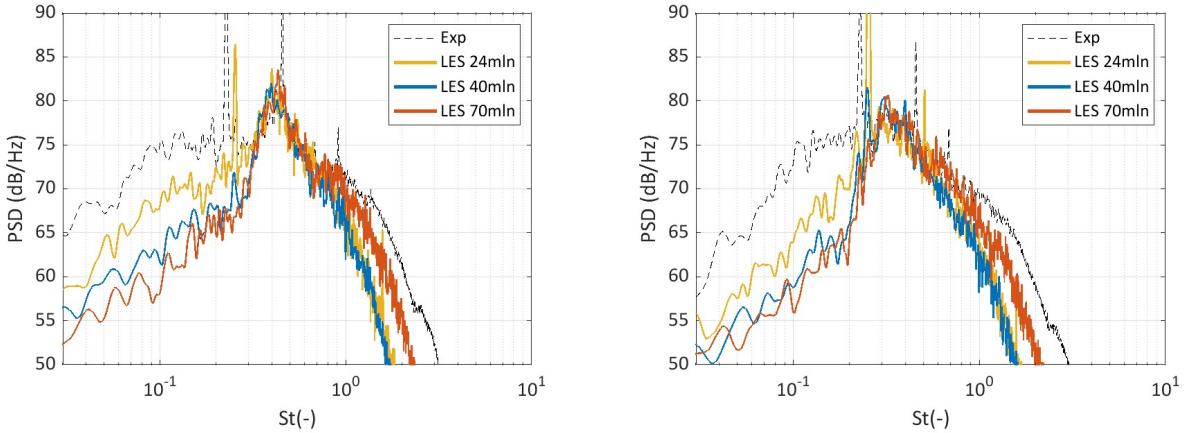

FIG. 13. Comparison of the Power Spectra Density predictions of the LES-FW-H model on three different grid resolutions with the LTRAC experiment for the NPR = 4.2 at 90° (a) and 120° (b) observer angles.

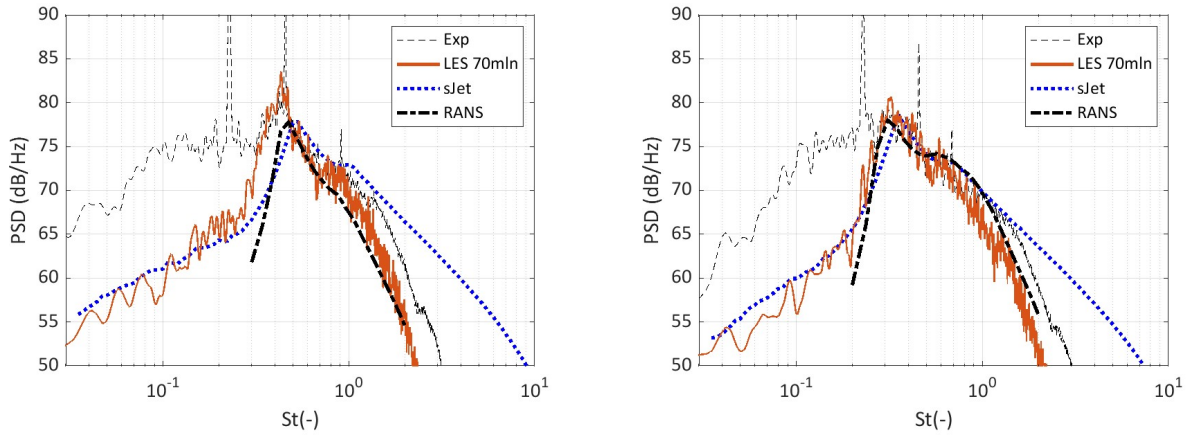

FIG. 14. Comparison of the Power Spectra Density predictions of the LES-FW-H and RANS-based acoustic models with the NASA sJet model and the LTRAC experiment for the NPR = 4.2 at 90° (a) and 120° (b) observer angles.

III. CONCLUSION

The flow and noise predictions of the two strongly under-expanded jets issuing from a high area ratio convergent nozzle corresponding to the LTRAC experiment at Monash University are obtained using Large Eddy Simulation (LES) and Reynolds Averaged Navier-Stokes (RANS) methods. The LES is based on the high-resolution CABARET solver accelerated on Graphics Processing Units (GPUs) with asynchronous time stepping. The LES solution starts from the nozzle exit where the inlet boundary condition is imposed using the available Particle Image Velocimetry (PIV) data from the LTRAC experiment. For the far-field noise predictions, the LES solution is coupled with the Ffowcs Williams – Hawkings (FW-H) method based on a permeable control surface with multiple closing discs. The RANS model is based on solving the 3D-axisymmetric equations using the $\kappa-\omega$ SST turbulence model, which includes the compressibility corrections and accounts for the adverse pressure gradients typical of supersonic flows. For the far-field noise modelling with the RANS solution, two versions of the Morris and Miller (2010) model are

implemented: with and without accounting for the mechanism of sound scattering by the shock-cells in the definition of the acoustic correlation scale. As it turns out, both models converge to the same result for the LTRAC jets considered, which can be attributed to the screeching mechanism of these jets.

For sufficient grid resolution, the LES solution shows good agreement with the LTRAC PIV data for the time-averaged velocity fields with accurately capturing the shock-cell structure over the first 4 shock-cells for both the NPR = 3.4 and NPR = 4.2 jet case. In the latter case, the Mach disk region is also accurately captured. In comparison with the LES, the RANS solution is less accurate for resolving the shock-cell structure especially at the centreline of the high-speed NPR = 4.2 jet. However, the RANS model better predicts the turbulent kinetic energy distribution in the jet shear layers in comparison with the LES solution, which over-predicts the turbulent kinetic energy levels. The reason for the turbulence intensity amplification could be due to the insufficient resolution of the LES solution and also the initially laminar turbulent inflow condition effect. Hence, future work will involve further LES grid refinement studies and imposing a synthetic turbulence inflow condition upstream of the nozzle exhaust. The current predictions of the LES-FW-H models are within 1-2dB from the RANS-based shock-associated noise model predictions and within 2-3dB from the LTRAC experiment over the high frequency range $0.6<St<2$, which is sufficiently above the frequencies influenced by jet noise. For low-frequencies ($0.04<St<0.5$), where the LTRAC data are contaminated by noise, the LES-FW-H solution is within 2-3dB from the sJet solution, which is based on empirical laws stemming from NASA jet noise database.

In addition, the LES solution correctly captures the screech tone frequencies of the experiment at St = 0.6 and St= 0.9 for the 90° noise spectrum of the NPR = 3.4 LTRAC jet and also those at St = 0.2 and St = 0.9 for the 120° spectrum of the same jet. Furthermore, the LES-FW-H solution of the NPR=4.2 LTRAC jet resolves the screech tone frequency of St=0.4 for both the 90° and 120°

observer angles. Notably, as the LES grid resolution increases in accordance with the grid count increase from 24 million to 70 million cells, the noise spectra predictions of the LES-FW-H model of the NPR = 4.2 jet consistently approach the LTRAC experimental spectra at high frequencies. The favourable comparison of the LES-FW-H results for the LTRAC jets with those obtained by the RANS-based acoustic analogy model within the range of frequencies relevant for Broad Band Shock Associated Noise suggests that the acoustic analogy approach remains an attractive tool for quick-turn-around-time evaluations of shock-associated jet noise.

ACKNOWLEGEMENTS

The research has been supported by the Engineering and Physical Sciences Research Council (EP/S002065/1), and the Russian Science Foundation (Grant No. 19-12-00256).

Sergey Karabasov acknowledges the study performed in TsAGI with the financial support provided by the Ministry of Science and Higher Education of the Russian Federation (Grant agreement of December 8, 2020 № 075-11-2020-023) within the program for the creation and development of the World-Class Research Center "Supersonic" for 2020-2025.

The authors are grateful to Prof. Daniel Edgington-Mitchell and Dr Dominic Tan for providing the LTRAC PIV and the acoustic measurement data and also to Dr Abbas Khavaran for sharing the sJet code.

REFERENCES

Bodony, D. J., Jaiyoung, R., Ray, P., Lele, S. K., (2006). "Investigating Broadband Shock-Associated Noise of Axisymmetric Jets Using Large-Eddy Simulation Investigating Broadband Shock-Associated Noise of Axisymmetric Jets Using Large-Eddy Simulation". 12th AIAA/CEAS Aeroacoustics Conference. doi: 10.2514/6.2006-2495.

Chintagunta, A, Naghibi, S.E., Karabasov S.A., (2018). "Flux-corrected dispersion-improved CABARET schemes for linear and nonlinear wave propagation problems", Computers & Fluids 169, 111-128.

Chintagunta, A, Naghibi, S.E., Karabasov S.A., (2017). "Dispersion Improved CABARET for Computational Aeroacoustics", 23rd AIAA/CEAS Aeroacoustics Conference.

Cowart, R., (2013). "Proceedings of Meetings on Acoustics", Montreal, Canada. doi: 10.1121/1.4800343.

Davies, P. O. A. L., Fisher, M. J. and Barratt, M. J., (1962). "The characteristics of the turbulence in the mixing region of a round jet", Journal of Fluid Mechanics, 15(3), pp. 337–367.

Edgington-Mitchell, D. M., Oberleithner, K., Honnery, D. R., and Soria, J., (2014). "Coherent structure and sound production in the helical mode of a screeching axisymmetric jet," Journal of Fluid Mechanics, Vol. 748, 822–847.

Faranosov, G. A., Goloviznin, V. M., Karabasov, S. A., Kondakov, V. G., Kopiev, V. F., and Zaitsev, M. A., (2013) "CABARET method on unstructured hexahedral grids for jet noise computation," Computers & Fluids, Vol. 88, pp. 165–179.

Ffowcs Williams, J.E. and Hawkings D. L., (1969) "Sound Generation by Turbulence and Surfaces in Arbitrary Motion", Philosophical Transactions of the Royal Society of London. Series A, Mathematical andPhysical Sciences, Vol. 264, No. 1151, 321-342.

Ghahramani, S., (2005). "Fundamentals of Probability, with Stochastic Processes", Edited by 3rd Edition. Massachuettes: Pearson.

Goloviznin, V. M., Samarskii, A. A., (1998). "Finite difference approximation of convective transport equation with space splitting time derivative", Jour Matem. Mod., 10(1), 86–100.

Goloviznin, V.M., Zaitsev, M.A., Karabasov, S.A., Korotkin, I.A., (2013). "New CFD algorithms for multiprocessor computer systems", Mosk. Gos. Univ, Moscow.

Harper-Bourne, M. and Fisher, M. J., (1973). "The Noise from Shock Waves in Supersonic Jets", AGARD Conference on Noise Mechanisms. Brussels: AGARD Conference on Noise Mechanisms, pp. 1–13.

Harper-Bourne, M., (2003). "Jet noise turbulence measurements", AIAA-2003-3214, 9th AIAA/CEAS Aeroacoustics Conference.

Kalyan, A, Karabasov, S.A., (2017). "Broad band shock associated noise predictions in axisymmetric and asymmetric jets using an improved turbulence scale model", Journal of Sound and Vibration, Volume 394, 28 April 2017, 392-417.

Karabasov, S.A., and Goloviznin, V.M., (2009). "Compact Accurately Boundary Adjusting high-REsolution Technique for Fluid Dynamics", J. Comput. Phys., 228, 7426-7451.

Khavaran, A, and Bridges, J., (2009a). "SHJAR Jet Noise Data and Power Spectral Laws", NASA/TM—2009-215608, http://gltrs.grc.nasa.gov, March 2009.

Khavaran, A., and Bridges, J., (2009b.) "Development of Jet Noise Power Spectral Laws Using SHJAR Data", AIAA J. 3378.

Lighthill, M. J., (1952). 'On Sound Generated Aerodynamically. I. General Theory', Proceedings of the Royal Society A: Mathematical, Physical and Engineering Sciences, 211(1107), pp. 564–587. doi: 10.1098/rspa.1952.0060.

Lighthill, M. J., (1954). 'On Sound Generated Aerodynamically. II. Turbulence as a Source of Sound', Proceedings of the Royal Society A: Mathematical, Physical and Engineering Sciences, 222(1148), pp. 1–32. doi: 10.1098/rspa.1954.0049.

Markesteijn A.P. and Karabasov S.A., (2019). "Simulations of co-axial jet flows on Graphics Processing Units: the flow and noise analysis", Royal Soc. Philosophical Transactions A. vol. 377, (2159).

Markesteijn, A.P. and Karabasov, S.A. (2018a). "GPU CABARET Solutions for the CoJeN Jet Noise Experiment", 2018 AIAA/CEAS Aeroacoustics Conference, AIAA AVIATION Forum, (AIAA 2018-3921).

Markesteijn, A.P. and Karabasov, S.A. (2018b). "CABARET solutions on Graphics Processing Units for NASA jets: grid sensitivity and unsteady inflow condition effect", CR Mecanique (Proc. French Academy of Sciences).

Markesteijn, A. P., Gryazev, V., Karabasov, S. A., Ayupov, R. S., Benderskiy, L. A., and Lyubimov, D. A., (2020) "Flow and Noise Predictions of Coaxial Jets," AIAA Journal, Vol. 58, No. 12, pp.5280-5293

Markesteijn, A.P., Semiletov, V.A., Karabasov, S.A., Tan, D.J., Wong, M., Honnery D. and Edgington-Mitchell, D. M., (2017). "Supersonic Jet Noise: an Investigation into Noise Generation Mechanisms using Large Eddy Simulation and High-Resolution PIV Data", AIAA 2017-3029.

Miller, S. A. E., (2013). "Towards a Comprehensive Model of Jet Noise using an Acoustic Analogy and Steady RANS Solution", in 19th AIAA/CEAS Aeroacoustics Conference. Berlin: American Institute of Aeronautics and Astronautics, pp. 1–27. doi: 10.2514/6.2013-2278.

Mitchell, D. M., Honnery, D. R., and Soria, J., (2013). "Near-field structure of underexpanded elliptic jets," Experiments in fluids, Vol. 54, No. 7, pp. 1–13. doi:10.1007/s00348-013-1578-3.

Morris, P. J. and Miller, S. A. E., (2010). "Prediction of Broadband Shock-Associated Noise Using Reynolds-Averaged Navier-Stokes Computational Fluid Dynamics," AIAA Journal 48(12):2931-2944. https://doi.org/10.2514/1.J050560

Pack, D. C., (1950). A note on Prandtl's formula for the wave length of a supersonic jet, Quarterly Journal of Mechanics and Applied Mathematics. doi: 10.1093/qjmam/3.2.173.

Paliath, U. and Morris, P. J., (2005). 'Prediction of Jet Noise From Circular Beveled Nozzles', in 11th AIAA/CEAS Aeroacoustics Conference. Monterey: American Institute of Aeronautics and Astronautics, pp. 23–25. doi: 10.2514/6.2005-3096.

Pérez Arroyo, C., Daviller, G., Puigt, G., Airiau, C., Moreau, S. (2019a). "Identification of temporal and spatial signatures of broadband shock-associated noise," Shock Waves., Vol. 29, 117-134. doi:10.1007/s00193-018-0806-4.

Pérez Arroyo, C., Moreau, S., (2019b). "Azimuthal mode analysis of broadband shock-associated noise in an under-expanded axisymmetric jet," Journal of Sound and Vibration, Vol. 449, , pp. 64–83. doi: https://doi.org/10.1016/j.jsv.2019.02.032.

Pineau, P., Bogey, C., Mach., (2019). "Waves near supersonic jets: study of azimuthal structure and generation process using conditional averages", JFM 10.

Powell, A. (1956) "Structural Fatigue Due to Jet Noise", The Journal of the Acoustical Society of America. Acoustical Society of America, 28(4), p. 782. doi: 10.1121/1.1905133.

Semiletov, V.A. and Karabasov, S.A., (2018). "A volume integral implementation of the Goldstein generalised acoustic analogy for unsteady flow simulations". Journal of Fluid Mechanics Vol. 853, 461-487. https://doi.org/10.1017/jfm.2018.572

Semiletov, V.A., and Karabasov, S.A., (2013). "CABARET scheme with conservation-flux asynchronous time-stepping for nonlinear aeroacoustics problems", Journal of Computational Physics, 253(15), 157165. https://doi.org/10.1016/j.jcp.2013.07.008

Semiletov, V.A., Yakovlev P.G., Karabasov, S.A., Faranosov, G.A. Kopiev, V.F., (2016a). "Jet and jet–wing noise modelling based on the CABARET MILES flow solver and the Ffowcs Williams–Hawkings method", International Journal of Aeroacoustics 15 (6-7), 631-645. https://doi.org/10.1177/1475472X16659387

Semiletov, V. A., Yakovlev, P. G., Karabasov, S. A., Faranosov, G. A., and Kopiev, V. F., (2016b) "Jet and jet–wing noise modelling based on the CABARET MILES flow solver and the Ffowcs Williams–Hawkings method," International Journal of Aeroacoustics, Vol. 15, No. 6-7, pp. 631–645. https://doi.org/10.1177/1475472X16659387

Shur, M. L., Spalart, P. R., Strelets, M. Kh., (2005). "Noise Prediction for increasingly complex jets. Part I: Methods and tests. Part II: Applications" Int. J. Aeroacoustics., 4(34), 21366.

Shur, M., Spalart, P., Streletsand, M., Garbaruk, A., (2006). "Further Steps in LES-Based Noise Prediction for Complex Jets", in 44th AIAA Aerospace Sciences Meeting and Exhibit. Reno: AIAA Aerospace Sciences Meeting and Exhibit, pp. 1–26. doi: 10.2514/6.2006-485.

Tam, C. K. W. and Auriault, L., (1999). "Jet mixing noise from fine-scale turbulence", AIAA Journal. American Institute of Aeronautics and Astronautics, 37(2), pp. 145–153. https://doi.org/10.2514/2.691

Tam, C. K. W. and Chen, K. C., (1979). "A statistical model of turbulence in two-dimensional mixing layers" Journal of Fluid Mechanics. 2006/04/19. Cambridge University Press, 92(2), pp. 303–326. doi: DOI: 10.1017/S002211207900063X.

Tam, C. K. W. and Jackson, J. A., (1986). "A multiple-scales model of the shock-cell structure of imperfectly expanded supersonic jets", Journal of Fluid Mechanics, 153, pp. 123–149. https://doi.org/10.1017/S0022112085001173

Tam, C. K. W. and Tanna, H. K., (1982). "Shock associated noise of supersonic jets from convergent-divergent nozzles", Journal of Sound and Vibration, 81(3), pp. 337–358. doi: 10.1016/0022-460X(82)90244-9.

Tam, C. K. W., (1975). 'Supersonic jet noise generated by large scale disturbances', Journal of Sound and Vibration, 38(1), pp. 51–79. https://doi.org/10.2514/6.1973-992

Tam, C. K. W., (1987). "Stochastic model theory of broadband shock associated noise from supersonic jets", Topics in Catalysis. Academic Press Inc. (London) Limited, 116(2), pp. 265–302. doi: 10.1016/S0022-460X(87)81303-2.

Tan, D.J., Wong, M., Honnery, D., Edgington-Mitchell, D., Kalyan, A., Gryazev, V., Markesteijn, A.P., Karabasov, S.A., Semiletov, V.A., (2016) "Supersonic Axisymmetric Jet Noise Collaboration, Report"

Tan D.J., Honnery, D., Kalyan, A., Gryazev, V., Karabasov, S.A., Edgington-Mitchell, D., (2019a), "Equivalent Shock-Associated Noise Source Reconstruction of Screeching Under-expanded Unheated Round Jets", AIAA Journal: 57(3), 1-15. https://doi.org/10.2514/1.J057400

Tan D.J., Honnery, D., Kalyan, A., Gryazev, V., Karabasov, S.A., Edgington-Mitchell, D., (2019b) "Correlation Analysis of High-Resolution Particle Image Velocimetry Data of Screeching Jets", AIAA Journal, 57, 735-748. https://doi.org/10.2514/1.J057041.

Tucker, P.G. and Karabasov, S.A., (2009). "Unstructured grid solution of the eikonal equation for acoustics". International Journal of Aeroacoustics, Vol. 8(6) 535-553. https://doi.org/10.1260/147547209789141498

van Dyke, M., (1975). Perturbation Methods in Fluid Mechanics. Parabolic Press. doi: 10.1017/S0022112077210226.

Zorumski, W. E. (1982a) Aircraft noise prediction program. Theoretical manual. Part 1. NASA TM 83199.

Zorumski, W. E. (1982b) Aircraft noise prediction program. Theoretical manual. Part 2. NASA TM 83199.